Revista Brasileira de Meteorologia, v.17, n.1, 19-33, 2002

TRANSPORT OF QUASI-GEOSTROPHIC POTENTIAL VORTICITY AND ITS USE IN SIMPLE CLIMATE MODELS

SERGIO H. FRANCHITO, V. BRAHMANANDA RAO, J. PABLO R. FERNANDEZ, AND S. R. CHAPA
Centro de Previsão de Tempo e Estudos Climáticos-CPTEC,
Instituto Nacional de Pesquisas Espaciais-INPE,
12201-970, São José dos Campos-SP, Brasil
fran@cptec.inpe.br

ABSTRACT

Quasi-geostrophic potential vorticity (PV) transport and Eliassen-Palm (EP) flux cross sections are examined for the Northern (NH) and Southern (SH) Hemispheres based on the NCEP/NCAR reanalysis data. The seasonal march of EP flux and EP divergence (and consequently PV transport) indicates that they increase from summer to winter in both the hemispheres. In general, the cross sections of EP divergence are similar to those presented in earlier studies for NH. The largest differences occur near the surface where the region of convergence of EP (positive PV transport) near the surface is shallower compared to the earlier studies. However, our results for SH are opposite to those obtained previously, which showed that EP divergence contours in summer are larger than in winter. This may be due the use of high qualitiy data in the present study while in the earlier studies station data (with coarser resolution and geographically not well distributed in SH) were used.

Exchange coefficients for PV transport calculated from the reanalysis data are used in a two-layer quasi-geostrophic statistical-dynamical model. The results show that the use of the exchange coefficents obtained from the reanalysis data improves the model results, mainly in the case of the simulation of zonal winds.

Key words: Quasi-geostrophic potential vorticity, simple climate models, Eliassen-Palm fluxes.

RESUMO: Transporte de vorticidade potencial quase-geostrófica e seu uso em modelos climáticos simples.

Transporte de vorticidade potencial quase-geostrófica (VP) e seções verticais do fluxo de Eliassen-Palm (EP) são estudados para os Hemisférios Norte (HN) e Sul (HS) baseando-se nos dados da reanálise do NCEP/NCAR. A marcha sazonal do fluxo de EP e divergência de EP (e, conseqüentemente, transporte de VP) indicam um aumento dos mesmos do verão para o inverno em ambos os hemisférios. No geral, as seções verticais da divergência de EP são similares àquelas apresentadas em estudos anteriores para o caso do HN. As maiores diferenças ocorrem próximo à superfície, onde a região de convergência de EP (transporte positivo de VP) é mais rasa em comparação com os estudos anteriores. Contudo, nossos resultados são opostos àqueles obtidos anteriormente para o caso do HS, os quais mostraram que a divergência dos contornos de EP no verão era maior que no inverno. Isto deve ser devido ao uso de dados de alta qualidade no estudo presente, enquanto, nos estudos anteriores dados de estação (com resolução mais grosseira e geograficamente mal distribuídos no HS), foram usados.

Coeficientes de troca para o transporte de VP calculados a partir dos dados da reanálise foram usados em um modelo estatístico-dinâmico quase-geostrófico de duas camadas. Os resultados mostraram que o uso dos coeficientes de troca obtidos, usando os dados da reanálise, melhorou os resultados do modelo, principalmente no caso da simulação dos ventos zonais.

Palavras-chave: transporte de vorticidade potencial quase-geostrófica, modelos climáticos simples, fluxos de Eliassen-Palm.

1. INTRODUCTION

Parameterizations of meridional transport of heat and momentum fluxes are essential in climate modeling. Climate models based only on the radiative equilibrium reproduce a superadiabatic and superbaroclinic atmosphere. So, there is a need to parameterize accurately the meridional transports of heat and momentum to obtain a more realistic simulation of climate. Parameterization of sensible heat transport has been done by using an exhange coefficient (Adem 1962, Green 1970,

Stone and Miller 1980). Parameterization of momentum transport is much less straightforward because the observed momentum transport in general is upgradient. An alternative way to parameterize momentum transport is connecting the momentum flux to the heat and quasi-geostrophic potential vorticity (PV) fluxes. Since the observed quasi-geostrophic PV transport is in general downgradient it is possible to parameterize the momentum transport indirectly through the use of exhange coefficients for quasi-geostrophic PV.

Evaluation of quasi-geostrophic PV transport and the associated exchange coefficients was made initially by Wiin-Nielsen and Sela (1971) (hereafter called WS) using data of 1963 for the Northern Hemisphere (NH). They noted that the quasi-geostrophic PV transport was negative (southward) in almost all the troposphere, except in a layer near the surface. The maximum negative transport of PV was found between 400 hPa and 300 hPa around 70°N. Several authors have shown the usefullness of the parameterization of PV transport in climate modelling (Sela and Wiin-Nielsen 1971, Wiin-Nielsen and Fuenzalida 1975, Ohring and Adler 1978, Gutman et al. 1984, and many others). In these models, the exchange coefficients calculated by WS were employed in a quasi-geostrophic PV system. More recently, Franchito and Rao (1991) extended the work of WS including the Southern Hemisphere (SH) data also. They computed the PV transport in both the hemispheres using the data of the National Meteorological Center (NMC) (1977-1979) and found results similar to those of WS for the NH. However, in the case of the SH two centers of negative transport of PV were noted: one in the tropical upper troposphere and the other in the middle troposphere at high latitudes. They calculated the exchange coefficients for PV transport and used them in a quasi-geostrophic statistical-dynamical model (SDM). Since the dataset used in that work was based on an objective analysis of NMC it was dynamically more consistent compared to that used in the previous study of WS. However, use of reanalysis data should further improve the model simulation because a state-of-the-art model is used (Kalnay et al., 1996) in obtaining these data. In the earlier studies (Franchito and Rao, 1991; Gutman et al., 1984; Ohring and Adler, 1978) zonal winds, particularly at 750 hPa were not simulated well. As we shall see latter, use of reanalysis data improves zonal wind simulation at 750 hPa.

The meridional transport of PV seems to be an useful tool to compare the general circulation of the two hemispheres. PV transport corresponds to the divergence of EP flux (Edmon et al. 1980, Hoskins 1983). EP vectors provide information on the relative role of wave heat and momentum forcing and the Rossby wave energy propagation, and the contours of EP divergence indicate the net effect of waves on PV transport and zonal mean flow. Observed EP cross sections based on data for the NH (11-year average of NMC data and 5-year average from Oort and Rasmusson 1971) were presented by Edmon et al. (1980). They noted that the EP cross sections for the transient eddies resemble to a significant degree the simulated cross sections of nonlinear baroclinic waves (Simmons and Hoskins 1980). EP cross sections including the SH, based on data of Newell et al. (1972, 1974), were presented by Karoly (1982). He obtained similar results as those from Edmon et al. (1980) for the NH. However, much less seasonal variation was noted in the SH compared to the NH. He noted also that EP divergence contours in the middle troposphere are larger in summer than in the winter in the SH.

As can be noted from the foregoing discussion, the earlier studies regarding the parameterization of PV transport and the use of EP cross sections as a diagnostic tool for disturbances on zonal mean wind were based on data sources which did not include consistency checks. Reanalysis data from the National Centers for Environmental Predictions (NCEP)/National Center for Atmospheric Research (NCAR) are now avalaible for performing climate studies. These data are generated by the state-of-the-art model and are devoid of errors due to changes of model physics. Detailed description of the assimilation system and output are given by Kalnay et al. (1996). In the present work we use the NCEP/NCAR reanalysis data for studying the quasi-geostrophic PV transport in both the hemispheres and its relationships with the dynamics of transient baroclinic waves. We use PV transport-EP cross sections for understanding the differences in the seasonal variations of zonal mean winds in the two hemispheres. Another objective of the paper is to use the exchange coefficients for PV transport calculated from the reanalysis data in a quasi-geostrophic climate model in order to verify how they improve the model simulations.

2. TRANSPORT OF QUASI-GEOSTROPHIC PV AND EP CROSS SECTIONS

2.1 Data and Methodology

The method for calculating PV transport and exchange coefficients are given in detail by WS. The

transport of quasi-geostrophic PV can be calculated by:

$$(Q'v')_o = \frac{1}{a\cos\varphi}\frac{\partial[(u'v')_o \cos^2\varphi]}{\partial\varphi} - \frac{\partial[f_o R(v'T')_o / \sigma p]}{\partial p} \quad (1)$$

where u'v' and v'T' are the meridional transport of momentum and heat, respectively; R, the gas constant; p, the pressure; f_o, the Coriolis parameter at 45°N (S); φ, the latitude; and σ is the static stability parameter. The subscript "o" denotes the zonal average.

The PV transport can be parameterized in terms of exchange coefficients (K_Q):

$$(Q'v')_o = -K_Q \frac{\partial(Q)_o}{a\partial\varphi} \quad (2)$$

where the PV gradient is given by:

$$\frac{1}{a}\frac{\partial(Q)_o}{\partial\varphi} = \frac{2\Omega\cos\varphi}{a} - \frac{1}{a^2}\frac{\partial[\frac{1}{\cos\varphi}\frac{\partial(u)_o\cos\varphi}{\partial\varphi}]}{\partial\varphi} \quad (3)$$

and Ω is the angular velocity of the earth.

The theory and the use of EP cross sections as a diagnostic for disturbances on zonal mean wind are given in detail by Edmon et al. (1980) and Hoskins (1983). The quasi-geostrophic EP flux vector ($\vec{F}$) is given by:

$$\vec{F} = (F_\varphi, F_z) = \rho_s a\cos\varphi[-(u'v')_o, \frac{Rf}{HN^2}(v'T')_o] \quad (4)$$

where the symbols have the usual meaning.

If $\vec{F}$ is represented in a latitude-height grid, $\vec{F}$ will appear divergent when $\nabla.\vec{F} = 0$.

Edmon et al. (1980) overcame this problem defining $\vec{\mathfrak{I}} = 2\pi a\cos\varphi\,\vec{F}$ in this case, the pattern of arrows whose horizontal and vertical components are proportional to $\mathfrak{I}_\varphi$ and $\mathfrak{I}_z$ will look nondivergent if and only $\nabla.\vec{F}=0$. Thus, the arrows in EP cross-sections have the components:

$$\vec{\mathfrak{I}} = (\mathfrak{I}_\varphi, \mathfrak{I}_z) = \rho_s 2\pi a^2[-\cos^2\varphi(u'v')_o, \frac{Rf}{HN^2}\cos^2\varphi(v'T')_o] \quad (5)$$

In order to compute PV transport-EP cross sections, we use observational data of the meridional transport of momentum and heat, zonal wind and temperature for each calendar month for the 22-year period (1979-2000) obtained from the NCEP/NCAR reanalysis data. The data for each calendar month represent an average over twenty-two years. The data are given at levels: 1000, 925, 850, 700, 600, 500, 400, 300, 250, 200, 150 and 100 hPa and at 2.5° latitude intervals from pole to pole. Since we are interested in studying the transient baroclinic eddies, data of momentum and heat fluxes by transient eddies are used. PV transport and PV-gradient are calculated from expressions (1) and (3), respectively. These values are used in expression (2) in order to obtain K_Q.

2.2 Results

Figures 1a-b show the mean annual values of PV transport and gradient, respectively. As can be seen in Fig. 1a, the PV transport is negative over almost entire troposphere with exception of a shallow layer near the surface and a small region around 400 hPa in subtropical latitudes. The negative PV transport is predominantly downgradient, since the PV gradient is positive over most part of the atmosphere (Fig. 1b). The maxima in negative PV transport are found near 400 hPa at high latitudes in both hemispheres, and there is a tendency of another center of maximum PV transport in the upper troposphere in the SH (around 35°S).

In general, our results are similar to those obtained by WS and Franchito and Rao (1991). However, some differences are noted. As can be seen in Fig. 1a, the regions of positive PV near the surface are narrower (from 45°N to the North Pole and from 60°S to the South Pole) and shallower (from the surface to 900 hPa) compared to the previous studies (see Fig. 1 of WS and Fig. 1 of Franchito and Rao 1991). These positive PV fluxes are not upgradient because the PV gradient is small or negative (Fig. 1b). This configuration of PV transport has important implications for the dynamics of baroclinic waves because the change of direction of PV fluxes due to a shallow layer near the surface satisfies the requirements for baroclinic instability to occur in the troposphere (Charney and Stern 1962; Schneider and Dickinson 1974). A striking feature noted in Fig. 1 is the ocurrence of a region of high values of PV transport between 700-800 hPa around 70°-80°S which was not observed in previous works. This may be due to the presence of the Antarctic continent The differences between our results and those from WS and Franchito and Rao (1991) are due to the fact that we used a high quality dataset with higher resolution compared with them. Also, the dataset we used corresponds to a larger period compared to the previous works.

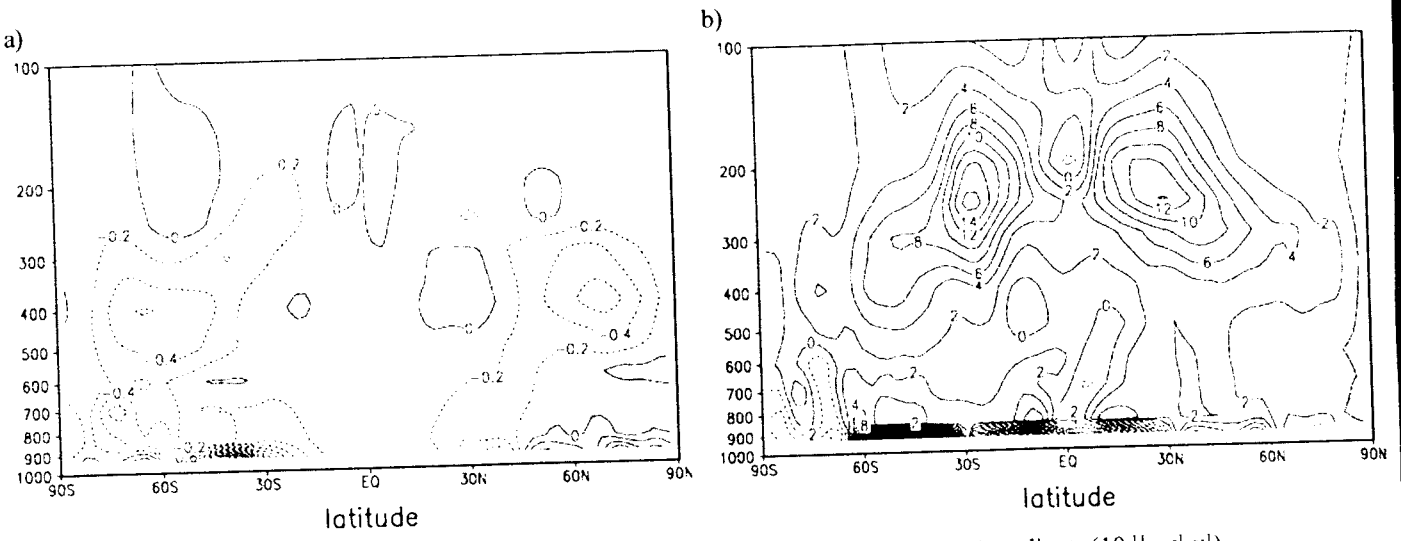

Fig. 1: Zonally-averaged mean annual: a) PV transport (10^{-4} m s^{-2}), and b) PV gradient (10^{-11} m^{-1} s^{-1}).

Figures 2a-d show the monthly mean values of PV transport for 3-month means: December-January-February (DJF), March-April-May (MAM), June-July-August (JJA) and September-October-November (SON), respectively. The spatial pattern of PV transport in these seasons is similar to the mean annual case. In all the months PV transport is negative throughout much of the troposphere, except in a thin layer near the surface and some regions in the middle and upper troposphere. The negative transport is predominantly downgradient since the PV gradient is positive in almost all the troposphere (Figs. 3a-d). The thin layer near the surface with positive PV fluxes corresponds to region where the PV gradient is negative or small, so that the PV transport is also downgradient The magnitude of PV transport is in general smaller in the present study compared to that obtained by Franchito and Rao (1991). Again, large differences occur near the surface where, as in the mean annual case.

The seasonal march of PV transport also shows large differences compared to that of Franchito and Rao (1991). In that work, PV transport was stronger in winter and weaker in summer in both the hemispheres. The maxima values of PV fluxes occurred in NH winter and PV transport was similar in the transition seasons. In the present study, PV transport increases from summer to winter in both the hemispheres. However, in NH PV fluxes are strong in all seasons, except in summer (DJF). In SH, PV transport increases from summer to winter (JJA) and decreases during spring (SON). During autumn (MAM), PV transport is stronger than during spring. As noted in Figs. 2a-d, the strongest PV transport is noted in SH winter. This is a striking difference between our results and those obtained by Franchito and Rao (1991).

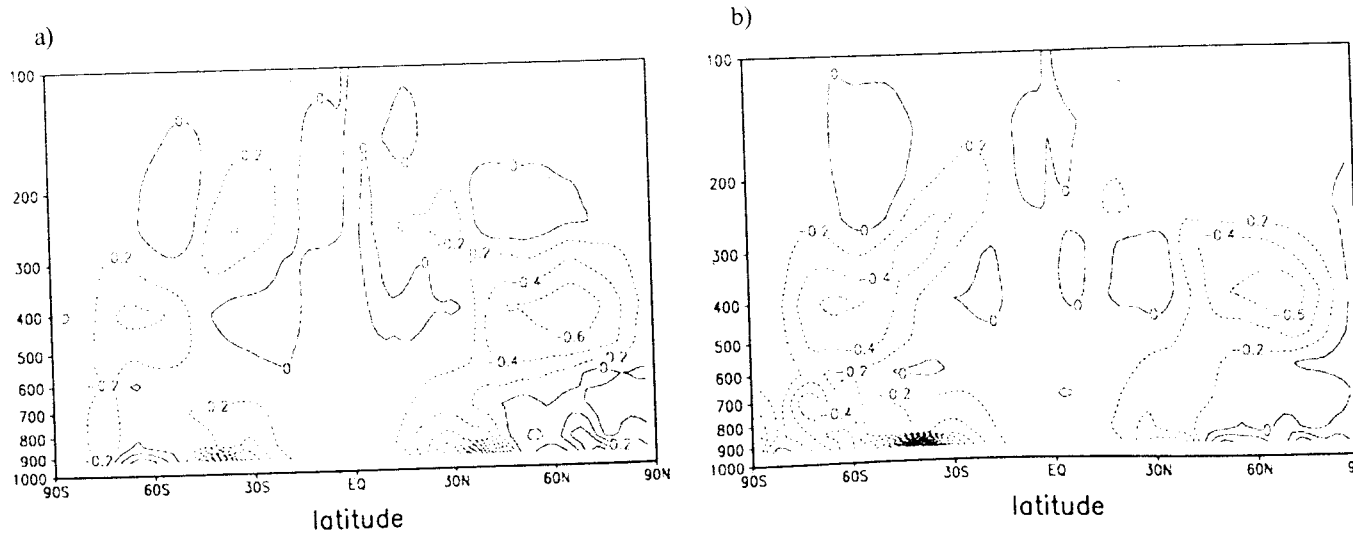

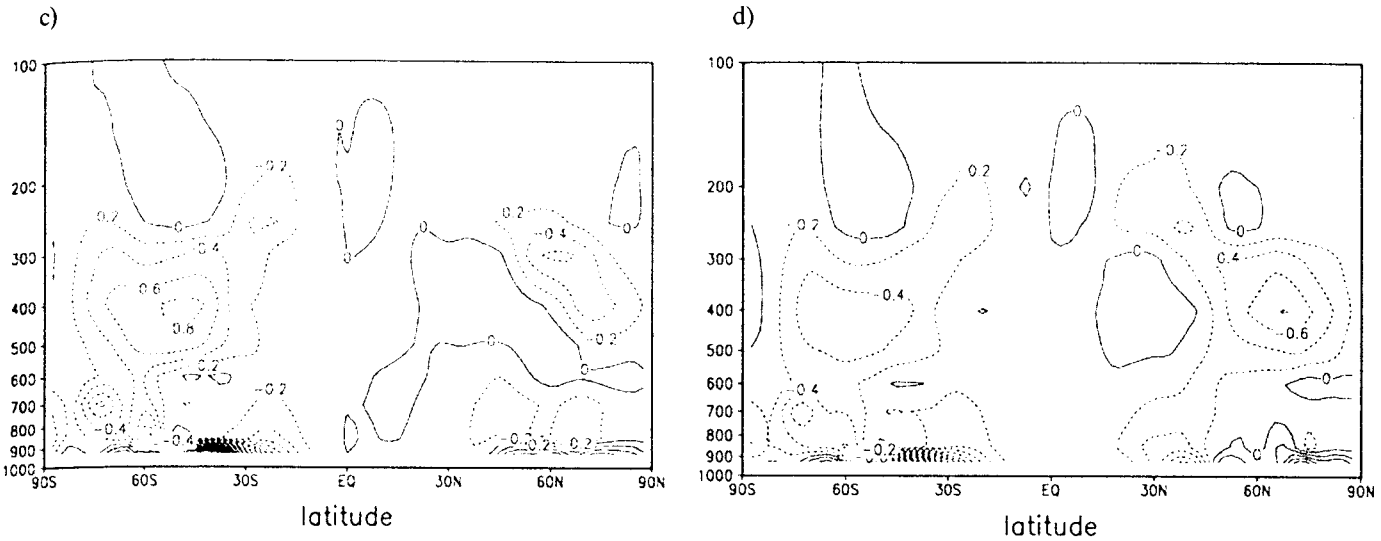

Fig. 2: Zonally-averaged PV transport for: a) DJF, b) MAM, c) JJA and d) SON. Units, 10^{-4} m s^{-2}.

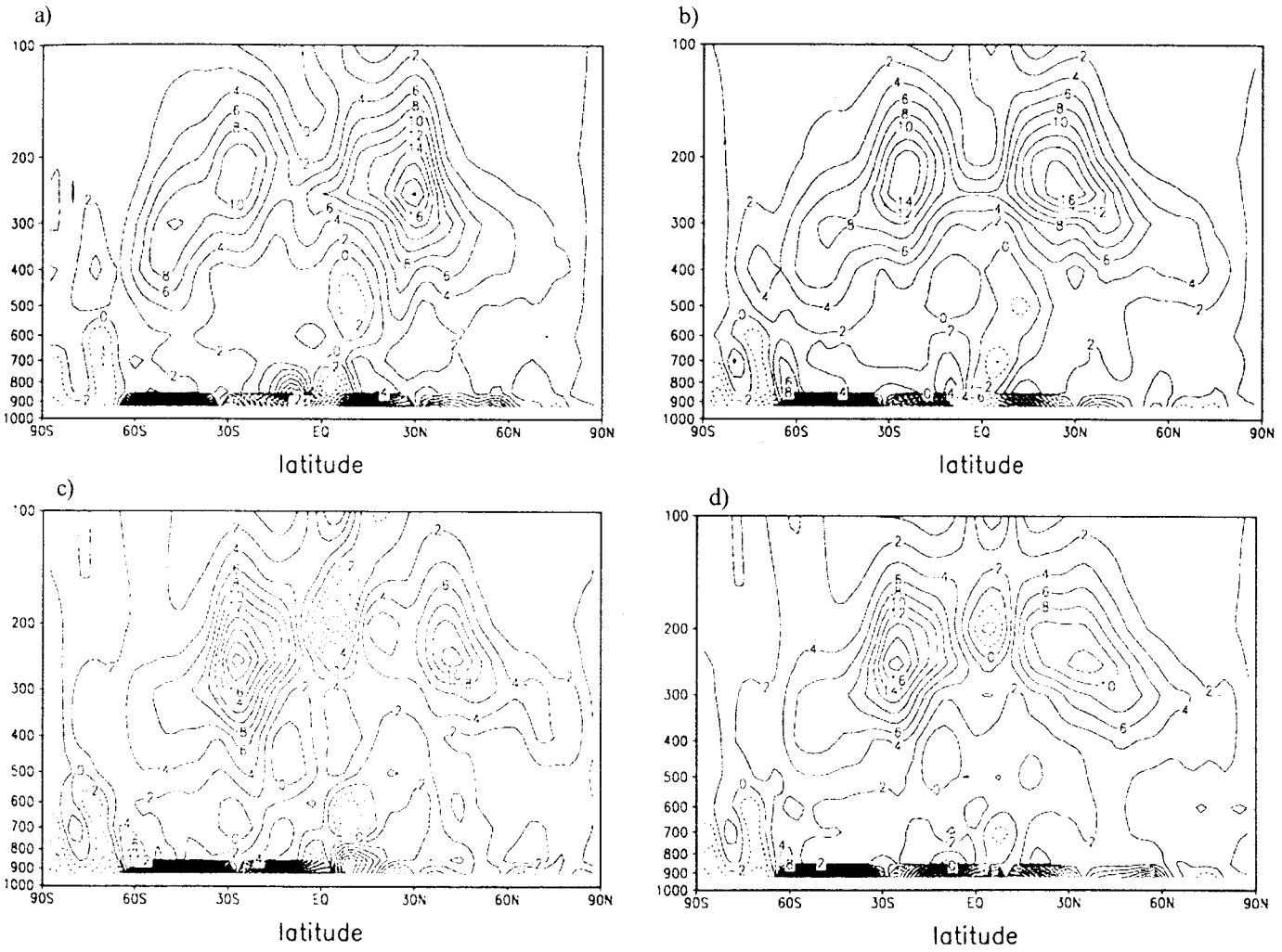

Fig. 3: Zonally-averaged PV gradient for: a) DJF, b) MAM, c) JJA and d) SON. Units, 10^{-11} m^{-1} s^{-1}.

Figures 4a-d show the EP cross sections for DJF, MAM, JJA and SON, respectively. As can be seen, there is EP convergence throughout much of the troposphere, which corresponds to downgradient PV fluxes in regions where PV gradient is positive (Figs. 2 and 3). The regions of EP divergence near the surface correspond to the thin layers where the PV transport is positive and PV gradient is negative, as commented earlier.

The configurations of EP cross sections showed in Fig. 4 are similar to those for the life-cycle averages of nonlinear baroclinic waves obtained from both the observational (Randel and Stanford 1985a, b) and model (Simmons and Hoskins 1980; Hoskins 1983) studies. The general patterns show that the heat fluxes dominate from the surface to the middle troposphere. Rossby wave group velocity propagation (given by EP vectors) is directed upwards away from the surface in the lowest levels. Above 500 hPa the EP vectors turn equatorward becoming nearly horizontal in upper levels. This equatorward propagation is associated with poleward momentum flux. EP convergence is noted in winter over almost entire troposphere, from 30°N (S) towards poles, and divergence of EP is found on the poleward side in the lower troposphere. The maxima (negative) values of EP contours occur around 400 hPa in both the hemispheres. The negative values of EP contours indicate that the waves tend to decelerate the zonal flow with zonal energy getting converted into wave energy. This configuration of EP cross sections is associated with northward PV flux at low levels and southward PV flux in the upper troposphere (Fig. 2). As can be noted in Figs. 4a-d, EP convergence and EP fluxes increase from summer to winter in both the hemispheres.

The spatial pattern of EP cross sections for DJF and JJA agrees in general with those in Edmon et al. (1980) and Karoly (1982). The magnitude of EP divergence calculated using the NCEP/NCAR data is higher than in the previous studies because the horizontal resolution of the reanalysis data is higher. As shown in Figs. 4a and 4c, EP divergence in the middle troposphere and EP fluxes in winter are larger than in summer. This is in agreement with the results of Edmon et al. (1980) and Karoly (1982) for the NH. However, in the case of the SH sensitive differences can be noted. Results of Karoly (1982) showed that in the middle troposphere EP divergence contours in summer were larger than in winter, which is opposite to our findings. Also, in his calculations the magnitude of EP flux in winter was slightly larger than in summer. In our case, larger differences between the values of EP flux from winter to summer are noted. These differences may be due to the different kind of data used in the two studies. While in the present study we used high quality reanalysis data for a long period (22 years) generated by the state-of-the-art model, in Karoly (1982) the data base for the zonal mean basic state and eddy statistics was station data for a short period (1957-1963) which were geographically not well distributted in SH. Also, the horizontal and vertical resolution of these data are coarser compared to the reanalysis data and data were not

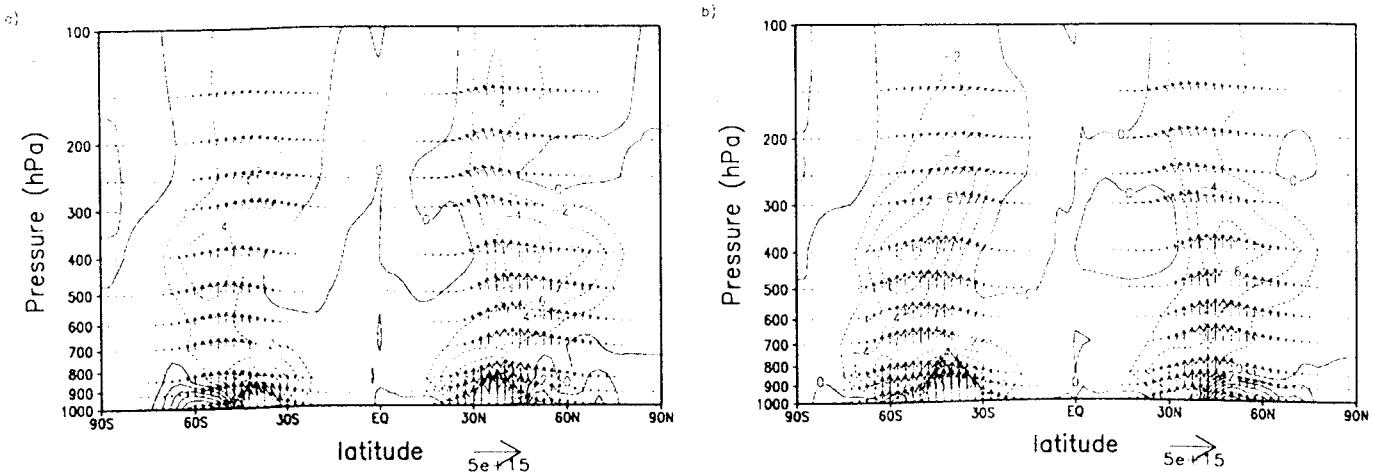

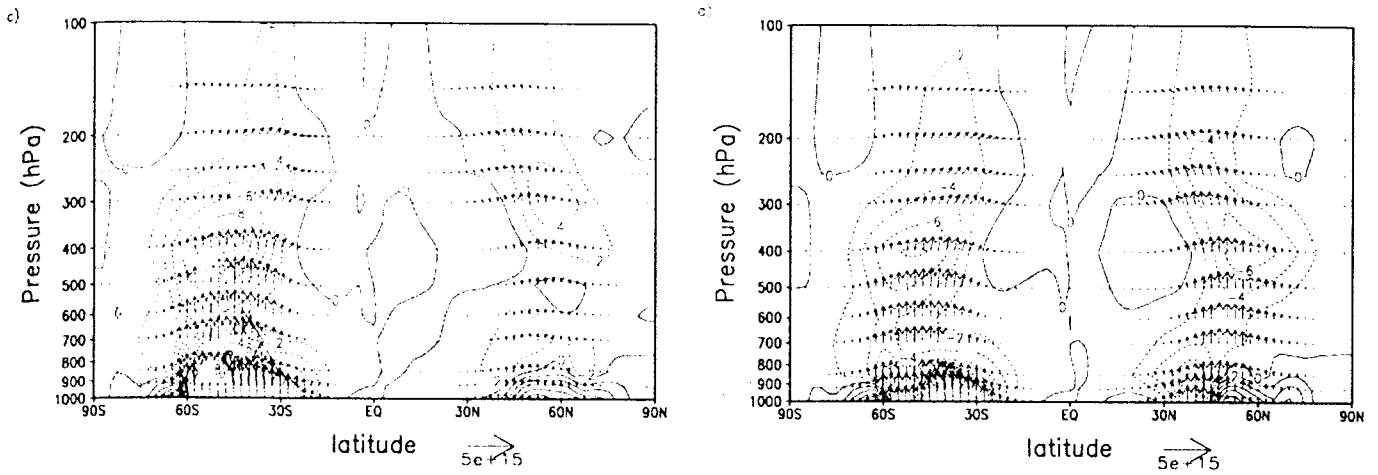

Fig. 4: Zonally-averaged EP cross sections for: a) DJF, b) MAM, c) JJA and d) SON. The contour interval is 5.0 x 10^{15} m^3. The horizontal arrow scale for EP flux in units of m^3 is indicated at bottom right.

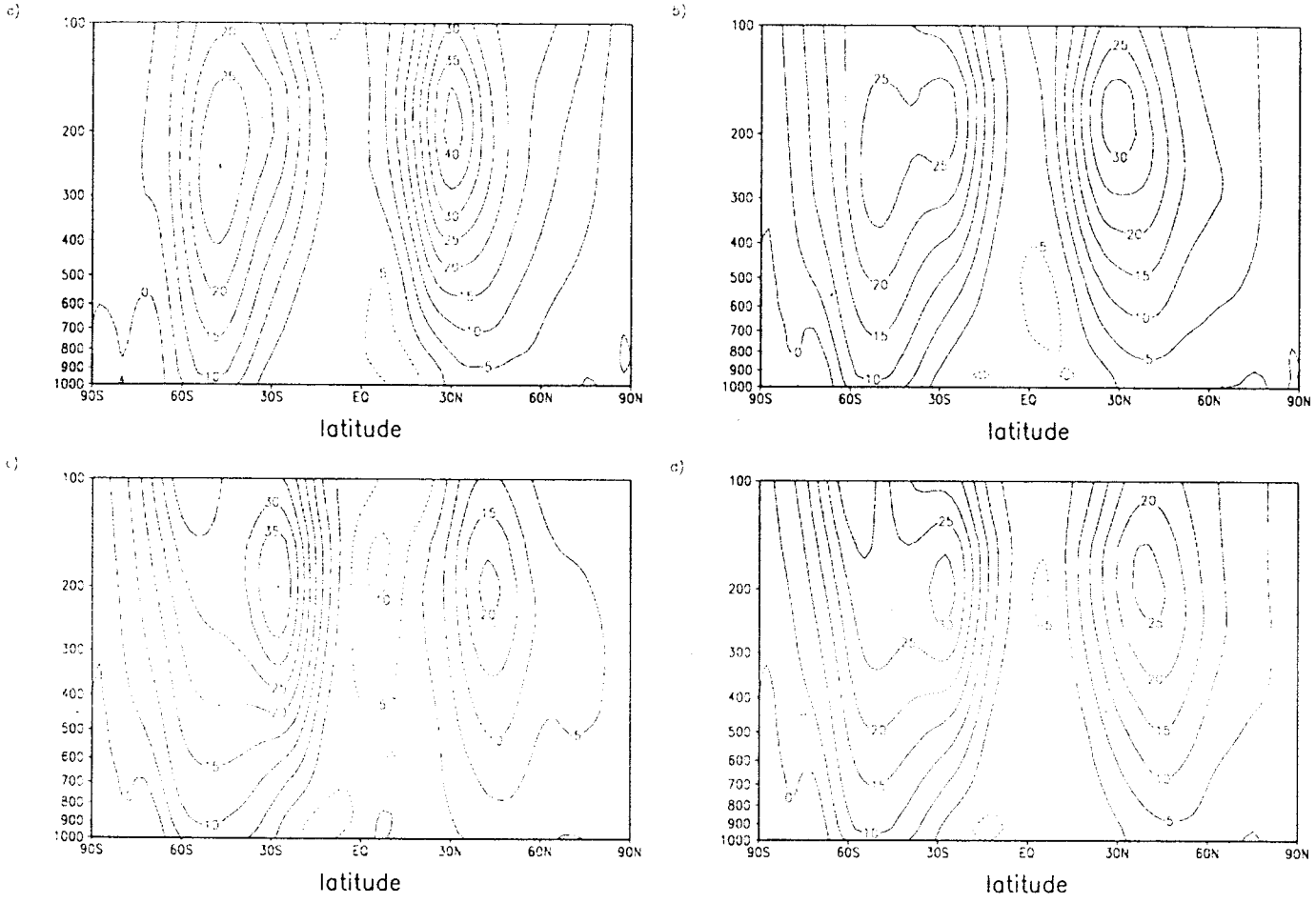

Fig. 5: Zonally-averaged zonall winds for a: a) DJF, b) MAM, c) JJA and d) SON. Units, m s^{-1}.

available at low levels in SH high latitudes.

The seasonal march of PV transport–EP cross sections are strongly related to the locations and magnitudes of the seasonal mean jet streams. Comparing Fig. 4 with Fig. 5, it can be noted that the maximum EP divergence in the upper troposphere occurs 5°-10° poleward of the corresponding monthly mean jet. This is in a good agreement with modeled baroclinic waves

(Hoskins 1983). As can be seen in Fig. 5, the mean jet in winter is stronger than in the other seasons in both the hemispheres. This is associated to the strongest EP fluxes and convergence of EP contours observed in this season. It is also noted that there is a tendency of two regions of maxima zonal winds in the SH in almost all the seasons. In DJF, a single jet is observed near 45°S. However, a tendency of bifurcation of the jet is noted between 30°-45°S. From summer to autumn, there is a bifurcation of the jet stream. In winter two regions of maxima zonal winds are observed near 30°S and 50°S around 200 hPa and 100 hPa, respectively. During spring there is a weaking of the zonal wind in the upper-troposphere and a single jet is observed in summer around 200–300 hPa. The seasonal variation of the jet stream in the SH is compatible with the configurations of PV transport and EP divergence contours (Figs. 2 and 4) which show a tendency of two maxima from summer to winter also. As can be seen in Fig. 5a, during the NH winter the maximum zonal wind occurs at 30°N near 200 hPa. However, a tendency of the occurrence of another region of maximum wind is noted near 50°N above 200 hPa. The tendency of two maxima zonal winds is not seen in the other seasons in the NH. As pointed by Lee (1999), the double jet is a typical feature of rotating atmospheres.

The zonal wind maxima is associated with the regions of higher baroclinicity. A suitable measure of the baroclinicity is provided by the Eady growth rate. This gives a diagnostic which can be used to link features of the mean temperature structure with transient eddy activity. Eady growth rate is defined by $\sigma = 0.31\ f/N\ |\partial u/\partial z|$ (Lindzen and Farrel, 1980), where: f is the Coriolis parameter; N, the Brunt-Vaisalla frequency; z, the upward vertical coordinate, and u is the zonal flow. Figures 6a-d show the Eady growth rate at 500 hPa for DJF, MAM, JJA and SON, respectively. As can be seen, σ is higher during the winter compared to the other seasons in both the hemispheres. The position of the zonal wind maxima is related to the highest values of Eady growth rate showed in Fig. 6. Comparing Figs. 5 and 6, it can be noted that the regions where Eady growth rate is higher correspond to the occurrence of maxima zonal winds. This is particularly true for the subtropical jet, where the zonal wind shear is maximum. For high latitudes, f becomes larger so that the higher values of Eady growth rate are shifted poleward compared to the positions of the secondary zonal wind maxima.

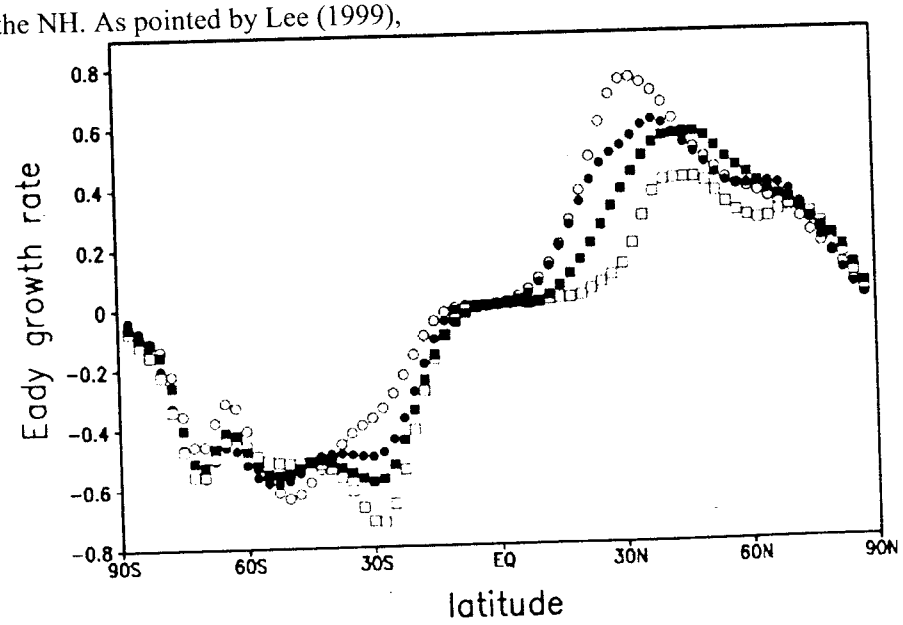

Fig. 6: Eady growth rate at 500 hPa for DJF (open circles), MAM (closed circles), JJA (open squares) and SON (closed squares). Values are in day^{-1}.

3. THE CLIMATE MODEL

In this section, the exchange coefficients for quasi-geostrophic PV transport computed from the reanalysis data using Equation 2 (Table 1) are used in a two-layer hemispheric quasi-geostrophic PV SDM similar to that developed by Sela and Wiin-Nielsen (1971). The prognostic equations of the model are:

$$\frac{\partial (Q_1)_o}{\partial t} = \frac{1}{a^2 \cos\varphi} \frac{\partial [K_{Q1} \cos\varphi\, \partial (Q_1)_o / \partial\varphi]}{\partial\varphi} - \frac{q^2 R (H_a)_o}{2 f_o c_p} - 2A(\zeta_T)_o$$

$$\frac{\partial (Q3)_o}{\partial t} = \frac{1}{a^2 \cos\varphi} \frac{\partial [K_{Q1} \cos\varphi \, \partial (Q3)_o / \partial\varphi]}{\partial\varphi} + \frac{q^2 R (H_a)_o}{2 f_o c_p} + 2A(\zeta_T)_o$$

$$-\varepsilon (\zeta_*)_o + 2\varepsilon (\zeta_T)_o$$

where $(Q_1)_o$ and $(Q_3)_o$ are the zonally averaged quasi-geostrophic PV at levels 1 (250 hPa) and 2 (750 hPa), respectively; $(H_a)_o$, the zonally averaged diabatic heating; K_{Q1} and K_{Q3}, the exchanges coefficients for the PV transport at 250 and 750 hPa, respectively; c_p, the specific heat for dry air; and A, q^2 and ε are constants. $(\zeta_*)_o$ and $(\zeta_T)_o$ are obtained by:

$$(\zeta_*)_o = \frac{[(Q_1)_o + (Q_3)_o]}{2} - f \qquad (8)$$

and

$$(\zeta_T)_o = \frac{[(Q_1)_o - (Q_3)_o]}{2} - q^2 (\psi_t)_o \qquad (9)$$

where f is the Coriolis parameter and $(\psi_t)_o$ is the zonally averaged stream function, obtained by:

$$\frac{1}{a^2 \cos\varphi} \frac{\partial [\cos\varphi \, \partial (\psi_t)_o / \partial\varphi]}{\partial\varphi} - q^2 (\psi_t)_o = \frac{[(Q_1)_o - (Q_3)_o]}{2} \qquad (10)$$

The zonally averaged temperature at 500 hPa, and the zonally averaged zonal winds at 250 and 750 hPa are obtained, respectively by:

$$(\psi_t)_o = \frac{R(T_2)_o}{2 f_o} \qquad (11)$$

$$(u_1)_o = \frac{a}{\cos\varphi} \int_0^{\varphi} (\zeta_*)_o \cos\varphi \, d\varphi \qquad (12)$$

$$(u_3)_o = \frac{a}{\cos\varphi} \int_0^{\varphi} (\zeta_T)_o \cos\varphi \, d\varphi \qquad (13)$$

Table 1: Latitudinal values of the exchange coefficients for 250 hPa (K_{Q1}) and 750 hPa (K_{Q3}) computed from the NCEP/ NCAR reanalysis data. Units, 10^6 m^2 s^{-1}.

SH	80°	70°	60°	50°	40°	30°	20°	10°
K_{Q1}	0.43	1.24	0.08	0.14	0.27	0.23	0.21	0.21
K_{Q3}	1.33	2.94	1.24	0.84	1.05	1.82	0.89	0.89
NH	10°	20°	30°	40°	50°	60°	70°	80°
K_{Q1}	0.10	0.16	0.14	0.13	0.52	0.85	1.06	1.42
K_{Q3}	0.60	0.60	1.22	1.15	0.77	0.98	1.34	0.67

In the present model the parameterization of the diab atic heating is improved. We take into account the effects of shortwave and longwave radiation, small-scale convection, evaporation and latent heat condensation, and subsurface conduction while in the model of Sela and Wiin-Nielsen (1971) the diabatic heating was approximated using a Newtonian form. The parameterization of the radiative processes is based on Jentsch (1991) and adapted to a SDM by Franchito et al. (1998); the other components of the diabatic heating have the same formulations as those proposed by Saltzman and Vernekar (1971) except in the case of the latent heat of condensation whose parameterization is based on the method suggested by Gutman et al. (1984). Tables 2a-b indicates the various surface and atmospheric heating processes that are taken into account in the model. The model is run separately for NH and SH using a latitudinal grid interval of 10°. The initial condition is an isothermal

atmosphere at rest. An implicit time-integration scheme is used with a time step of 6 hours. The model is integrated for one year for obtaining stationary solutions.

In order to verify how the use of K_Q values obtained from reanalysis data improves the simulation of the zonally averaged variables the model is also run using K_Q values obtained earlier from the NMC data (Franchito and Rao 1991).

Figures 7a-c show the simulated and observed zonally averaged mean annual values of the temperature at 500 hPa, zonal winds at 250 hPa and 750 hPa, respectively. The observed data are obtained from the NCEP/NCAR reanalysis for the period 1960-94 (mean values for 35 years). Simulated values using K_Q from the NMC data are also shown. As can be seen in Fig. 7a, the latitudinal profile of the temperature at 500 hPa is well simulated by the model in both the cases using the K_Q from NCEP/NCAR reanalysis and NMC datasets. However, the simulation of $(T_2)_o$ is improved when K_Q values from reanalysis are used.The simulation of the zonal wind at 250 hPa is also improved when K_Q values from reanalysis data are used, except in the tropical region. As shown in Fig. 7b, the position and magnitude of the maximum in NH are in good agreement with the observations. In the SH, although the maximum is shifted poleward compared with the observations in both the cases, the magnitude of the maximum is better simulated when the K_Q values from the reanalysis data are used in the model. As in the case of the zonal wind at 250 hPa, the simulation of the zonal wind at 750 hPa is also improved when the model is run with K_Q from the reanalysis data, mainly in NH (Fig. 7c).

Table 2: Formulation of the surface (a) and atmospheric diabatic (b) heating used in the model. The symbols are defined in Appendix 1.

		Surface diabatic heating
i	H_s (i)	
1	Shortwave solar radiation	$R_o \tau (1 - r_s) / (1 - r_s r_a)$
2	Longwave radiation	$\sigma_B T_s^4 - [(1 - N) \mathcal{L}(H)\downarrow + N \mathcal{L}(h_b)\downarrow + N \sigma_B T_b^4 T(0, h_b)]$
3	Small-scale convection	$- [b (T_s - T_2) + c]$
4	Evaporation	$w [e H_s(3) + f]$
5	Subsurface heat flux	$- K (T_s - T_D)$

		Atmospheric diabatic heating
i	H_a (i)	
1	Shortwave solar radiation	$R_o \{ 1 - r_p - \tau [\tau r_s + (1 - r_s)] / (1 - r_a r_s) \}$
2	Longwave radiation	$\sigma_B T_s^4 - \sigma_B T_s^4 (1 - N) T(0, H) - N [\mathcal{L}(h_b)\downarrow + \mathcal{L}(h_t)\uparrow] - N [\sigma_B T_b^4 T(0, h_b) + \sigma_B T_t^4 T(h_t, H)] - (1 - N) [\mathcal{L}(H)\downarrow + \mathcal{L}(0)\uparrow]$
3	Small-scale convection	$- H_s(3)$
4	Latent heat flux	$- H_s(4) - L (a_4 \omega + a44)$, for $\varphi < 70°N$ (S) $- H_s(4) + g (N - N_m)$, for $\varphi > 70°N$ (S)

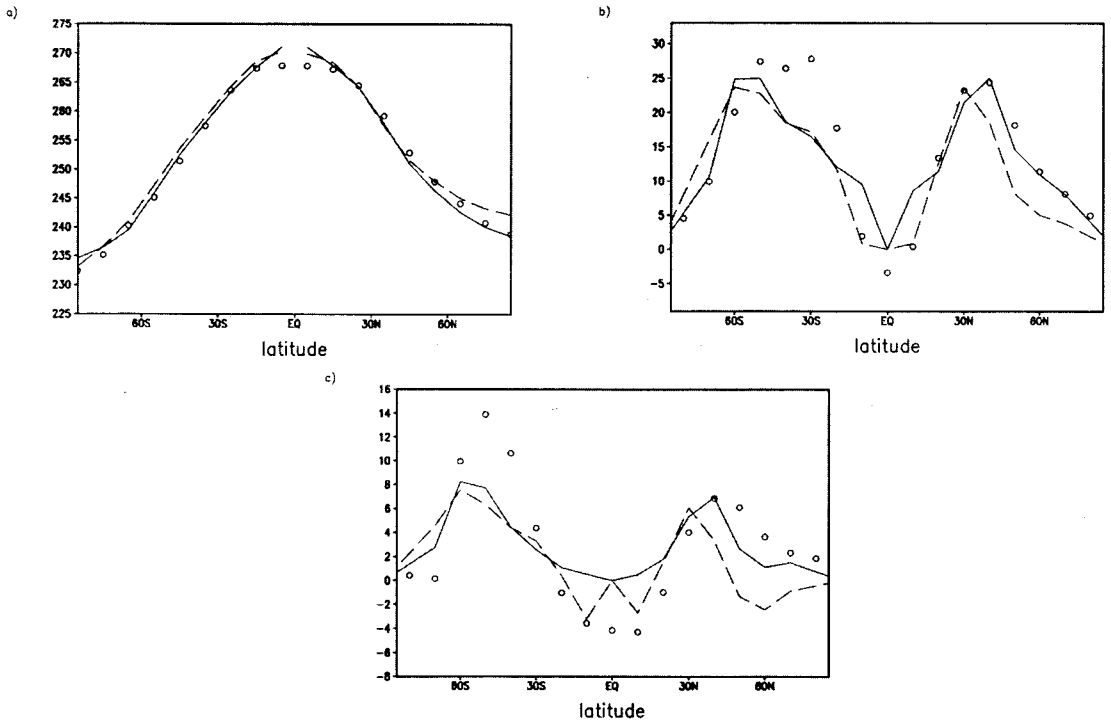

Fig. 7: Mean annual zonally-averaged: a) temperature at 500 hPa (K), b) zonal wind at 250 hPa (m s^{-1}) and c) zonal wind at 750 hPa (m s^{-1}). The full line corresponds to the model run using exhange coefficients calculated from NCEP/NCAR reanalysis data, the dashed line represents the model run with exhange coefficients computed from NMC data (Franchito and Rao, 1991) and the observations (mean values for 35 years from the NCEP/NCAR data) are indicated by open circles.

Tables 3-4 show the bias, rms, and absolute errors between the mean annual simulated and observed values of $(T_2)_o$, $(u_1)_o$ and $(u_3)_o$ for the NH and the SH, respectively, for the runs with K_Q from the reanalysis and NMC datasets. As can be seen, the bias, rms and absolute errors are smaller in both the hemispheres when K_Q from the reanalysis data is used in the model. As can be seen in Table 3 and 4, the improvement in the model simulations is higher in the case of the zonal winds. Lack of good agreement between the 750 hPa observed and simulated zonal wind values was one of the problems noted earlier (Franchito and Rao, 1991; Gutman et al., 1984; Ohring and Adler, 1978).

Table 3: Rmse, bias, and absolute error for the temperature at 500 hPa (K) and zonal winds at 250 hPa and 750 hPa (m s^{-1}) simulated by the model using exchange coefficients computed from reanalysis data and NMC data. Values are for the NH.

	$(T_2)_o$		$(u_1)_o$		$(u_3)_o$	
	Reanalysis	NMC	Reanalysis	NMC	Reanalysis	NMC
rmse	1.532	1.778	3.321	5.024	2.557	4.079
Bias	-0.421	0.748	0.028	-3.681	0.137	-2.045
Abs. Error	1.267	1.487	2.181	3.877	2.104	3.585

Table 4: Same as Table 3 but for the SH.

	$(T_2)_o$		$(u_1)_o$		$(u_3)_o$	
	Reanalysis	NMC	Reanalysis	NMC	Reanalysis	NMC
rmse	1.476	1.586	6.192	6.091	3.737	3.998
Bias	0.911	1.461	-1.664	-2.127	-0.763	-1.149
Abs. Error	1.155	1.461	5.117	5.439	3.208	3.162

The model used in the present study is a two-dimensional zonally-averaged SDM. This class of model occupies an intermediary position in the hierarchy of models. Although the SDMs are simpler than the most complete three-dimensional general circulation models (GCMs), they include a more sophisticated treatment of meridional processes compared to that in the one-dimensional energy balance models (EBMs). The EBMs treat only the thermodynamics of the climate system whereas the SDMs also treat meridional dynamics and hydrology also. The results presented above showed that $(T_2)_o$ is simulated well in both the cases using K_Q values obtained from the NMC and reanalysis datasets (although in the latter the model values are closer to the observations). This means that the energy balance at the surface is simulated well in both the cases. However, the simulation of the zonal winds (and consequently the model dynamics) is greatly improved when the K_Q values from the reanalysis data are used. Thus, the use of the computed K_Q values using the high quality reanalysis data contributes for a better treatment of meridional dynamical processes in a SDM.

4. SUMMARY AND CONCLUSIONS

In this paper PV transport-EP fluxes and their connections with baroclinic wave activities are studied. For this purpose, the NCEP/NCAR reanalysis data are

used. Seasonal variation and interhemispheric differences are discussed. The results showed that the configurations of EP cross sections are similar to those for life-cycle averages of nonlinear baroclinic waves obtained for both the observational (Randel and Stanford, 1985a-b) and model (Simmons and Hoskins 1980, Hoskins 1983) studies. In both the hemispheres EP flux convergence is noted over most of the troposphere, which corresponds to downgradient PV fluxes in regions where PV gradient is positive. The maxima of EP flux convergence occur in the upper troposphere. EP flux divergence is observed in a shallow layer near the surface. In this region PV fluxes are also downgradient because PV transport is positive and PV gradient is negative or small. This configuration of EP cross sections is associated strongly with northward PV fluxes at low levels and southward PV fluxes in the upper troposphere.

The analysis of seasonal march showed that in both the hemispheres EP fluxes and EP divergence (and consequently PV transport) are stronger in winter than in summer because of the higher baroclinicity in this season. Eady growth rate was calculated for each season, showing that the higher values occur in the winter. The results of the present work are in agreement with those from the previous studies for the NH. However, in the case of the SH significant differences are noted. Karoly (1982) noted that in the middle troposphere EP divergence contours in summer are larger than in winter, which is opposite to our results. Also, in his study the magnitude of EP fluxes in winter was sligthy larger than in summer, while in our case larger differences from summer to winter are observed. These differences may be due to the fact in the present work high quality reanalysis data for a long period is used while in Karoly (1982) poor quality dataset based on station data was used.

The seasonal march of PV transport and EP cross sections are strongly related to the location and magnitude of the monthly mean jets. The maximum EP divergence in the upper troposphere occurs 5°-10° poleward of the corresponding monthly mean jet. This agrees well with that of modeled baroclinic waves (Hoskins, 1983). The strongest zonal winds observed in winter in both the hemispheres are associated with the strongest EP fluxes and EP convergence in this season. The double jet in the SH winter is compatible with the configurations of PV transport and EP divergence which show a tendency of two maxima from summer to winter. In the NH, a double jet is not observed. However, there is a tendency of a secondary maximum zonal wind in winter. The position of the maxima zonal winds is in agreement with the highest values of Eady growth rate, mainly in the case of the subtropical jet, where the zonal wind shear is maximum. In high latitudes, since f becomes larger the region of higher values of Eady growth rate is shifted poleward compared to the secondary maximum zonal wind.

Exchange coefficients for PV transport are computed for both the hemispheres using the NCEP/ NCAR reanalysis data. A two-layer quasi-geostrophic model similar to that of Sela and Wiin-Nielsen (1971), but including improved parameterization of the diabatic heating, is applied to both the hemispheres. The results showed that the general characteristics of mean annual zonally-averaged temperature and zonal winds are reproduced reasonably well. The use of exchange coefficients computed using the reanalysis data improves the model results, mainly in the case of the zonal winds.

Appendix 1

Meaning of the symbols of the diabatic heating fluxes parameterization used in the SDM

a_4	constant equal to 0.1×10^{-5} m Pa^{-1} (HN) and 0.17×10^{-5} m Pa^{-1} (HS)
a_{44}	constant equal to 0.2×10^{-8} m s^{-1} (HS) and 0 (HN)
b, c, e, f, g	empirical constants independent of the latitude
h_b	height of the top of the cloud cover
h_t	height of the cloud cover base
H	height of the atmosphere (assumed equal to 10 km)
K	factor proportional to the conductive capacity of surface medium
L	latent heat of vaporization
N	cloudiness amount at a latitude belt
N_m	hemispheric average of the cloudiness amount
r_a	albedo of the atmosphere
r_s	surface albedo
R_o	solar radiation incident at the top of the atmosphere
T_b	radiation temperature at the cloud cover base
T_D	subsurface temperature
T_s	surface temperature
T_t	radiation temperature at the top of the cloud cover
T_2	temperature at 500 hPa
w	water availability
φ	Latitude
$L(z)\downarrow$	downward longwave flux at level z
$L(z)\uparrow$	upward longwave flux at level z
σ_B	Stefan-Boltzman constant
τ	transmissivity of the atmosphere
$?(z_1, z_2)$	transmission function between levels z_1 and z_2
ω	vertical velocity at 500 hPa

5. REFERENCES

ADEM, J. On the theory of general circulation of the atmosphere. **Tellus**, v.14, p 102-115, 1962.

CHARNEY, J. G.; STERN, M. On the stability of internal baroclinic jets in a rotating atmosphere. **J. Atmos. Sci.,** v.19, p.159-72, 1962.

EDMON, H. J.; HOSKINS, B. J.; MCINTYRE, M. E. Eliassen=Palm cross sections for the troposphere. **J. Atmos. Sci.,** v.37, p.2600-16. 1980.

FRANCHITO, S. H.; RAO, V. B. Quasi-geostrophic potential vorticity in the Northern and Southern Hemisphere and simple climate models. **J. Meteorol. Soc. Jpn.**, v.69, p.233-9. 1991.

FRANCHITO, S. H.; RAO, V. B.; SILVA, R. R. A parameterization of radiative fluxes suitable for use in a statistical-dynamical model. **Meteorol. Atmos. Phys.,** v.69, p.23-38, 1998.

GREEN, J. S. A. Transfer properpies of large-scale eddies and general circulation of the atmosphere. **Q. J. Roy. Meteorol. Soc.**, v.96, p.157-85, 1970.

GUTMAN, G.; OHRING, G.; JOSEPH, J. H. Interaction between the geobotanic state and climate: a suggested approach and a test a zonal model. **J. Atmos. Sci.,** v.41, p.2663-78, 1984.

HOSKINS, B. J. Modelling of the transient eddies and their feedback on the mean flow. In: Hoskins, B. J.; Pearce, R. (Ed). *Large-scale dynamical processes in the atmosphere.* Academic Press, 1983. 396p.

JENTSCH, V. An energy balance climate model with hydrological cycle 1: model description and sensitivity to internal parameters. **J. Geophys. Res.**, v.96, D9, p.16169-7179, 1991.

KALNAY, E. et al. The NCEP/NCAR 40 year reanalysis project. **Bull. Am. Meteorol. Soc.**, v.77, p.437-71., 1996.

KAROLY, D. J. Eliassen-Palm cross sections for the Northern and Southern Hemispheres. **J. Atmos. Sci.**, v.39, p.178-82, 1982.

LEE, S. Why are the climatological zonal winds easterly in the equatorial upper troposphere? **J. Atmos. Sci.**, v.56, p.1353-63.1999.

LINDZEN, R. S.; FARRELL, B. A simple approximate result for the maximum growthrate for baroclinic instabilities. **J. Atmos. Sci.**, v.37, p.1648-54, 1980.

NEWELL, R. E. et al. *The general circulation of the tropical atmosphere and interactions with extratropical latitudes.* The MIT Press, 1972. v.1, 258p.

NEWELL, R. E. et al. *The general circulation of the tropical atmosphere and interactions with extratropical latitudes.* The MIT Press, 1974. v.2, 371p.

OHRING, G.; ADLER, S. Some experiment with a zonally averaged climate model. **J. Atmos. Sci.**, v.35, p.186-205. 1978.

OORT, A. H.; RASMUSSON, E. M. *Atmospheric circulation statistics.* NOOA Prof. Pap. No. 5, Washington: U. S. Dept. Of Commerce, 1971. 323p.

RANDEL, W. J.; STANFORD, J. L. The observed life cycle of a baroclinic instability. **J. Atmos. Sci.**, v.42, p.1364-73,1985a.

RANDEL, W. J.; STANFORD, J. L. An observational study of medium scale wave dynamics in the Southern Hemisphere summer. Part I: Wave structure and energetics. **J. Atmos. Sci.**, v.42, p.1172-88, 1985.

SALTZMAN, B.; VERNEKAR, A. D. An equilibrium solution for the axially-symmetric components of the Earth's macroclimate. **J. Geophys. Res.**, v.76, p.1498-524, 1971.

SCHNEIDER, S. H.; DICKINSON, R. E. Climate Modeling. **Geophys. Space Phys.**, v.12, p.447-93, 1974.

SELA, J.; WIIN-NIELSEN, A. Simulation of the atmospheric annual energy cycle. **Mon. Wea. Rev.**, v.99, p.460-8. 1971.

SIMMONS, A. J.; HOSKINS, B. J. The lyfe cycles of some nonlinear baroclinic waves. **J. Atmos. Sci.**, v.35, p.414-32. 1980.

STONE, P. H.; MILLER, D. A. Empirical relations between seasonal changes in meridional temperature gradients and meridional fluxes of heat. **J. Atmos. Sci.**, v.37, p.1708-21, 1980.

WIIN-NIELSEN, A.; SELA, J. On the transport of quasi-geostrophic potential vorticity. **Mon. Wea. Rev.**, v.99, p.447-459, 1971.

WIIN-NIELSEN, A.; FUENZALIDA, H. On the simulation of the axisymmetric circulation of the atmosphere. **Tellus**, v.27, p.199-214. 1975.